



Cite this: *RSC Adv.*, 2017, 7, 29933

Received 24th April 2017

Accepted 25th May 2017

DOI: 10.1039/c7ra04532h

rsc.li/rsc-advances

Facile synthesis of novel CuCo_2S_4 nanospheres for coaxial fiber supercapacitors†

Qiufan Wang,^{ID} Xiao Liang, Depeng Yang and Daohong Zhang*

Flexible and highly efficient energy storage units act as one of the key components in portable electronics. In this work, based on CuCo_2S_4 nanospheres, a flexible all-solid-state coaxial fiber supercapacitor is designed and produced via a low cost and facile method. The as-fabricated flexible device exhibits high specific capacitance, high energy density, excellent rate capability and outstanding long-term cycling stability. This approach can be an efficient strategy for the preparation of novel and low-cost electrodes for various applications.

Introduction

Developing high-performance electrochemical energy storage devices has been one of the important issues in the energy strategic projects established by the governments of countries around the world.¹ Among various energy storage devices, rechargeable supercapacitors (SCs), with high power density, fast charge/discharge rate, and long lifespan, are considered typically as one of the most appropriate choices for energy storage and conversion.^{2,3} Especially, flexible SC, such as fiber SCs, and flexible micro-SC, have been devoted a significant amount of effort, owing to their potential applications in the fields of portable electronic devices. To achieve flexible SCs with comprehensive advantage requirements, such as high charge storage capability and mechanical flexibility is the greatest challenge,⁴ one of the most effective ways is to realize the perfect combination of bendable current collectors with good mechanical flexibility and electrode materials with a high capacitive performance. The commercial Ti wire own high conductivity and high flexibility. Fiber SC fabricated based on Ti wire can render the designer free from conventional constraints. Furthermore, the Ti wire based SC could be easily worn on human body, realization the practical wearable electronics.

Generally, the properties of SCs are influenced by the electrode material, electrolyte and assembly technology. Among them, the vital factor is electrode material, and therefore it has become a research focus for researchers. Transition metal oxides are widely considered as the most low cost, low toxicity, environmental friendliness, and multiple oxidation states. However, oxides usually have low electrical conductivity, which

limits their rate capability, another key parameter of supercapacitor.^{5,6} In contrast, metal sulfides have excellent chemical stability, rich valence,⁷⁻⁹ and better electrical conductivity.¹⁰⁻¹² Compared to the single-component metal sulfides, binary metal sulfides show richer redox reactions and higher electronic conductivity, resulting in the enhancement of the electrochemical performances. Dong *et al.* reported the fabrication of zinc cobalt sulfide ($\text{Zn}_{0.76}\text{Co}_{0.24}\text{S}$) nanoartichokes by co-decomposing Zn and Co precursors in a hot oleylamine/oleic acid solution through a facile oil phase approach, which obtained a capacitance of 486.2 F g^{-1} at 2 A g^{-1} .¹³ Xiao *et al.* reported the single crystalline nanotube arrays NiCo_2S_4 , which manifested higher specific capacitance and rate capability than NiCo_2O_4 .¹⁴ Yuan *et al.* fabricated hollow hetero- $\text{NiCo}_2\text{S}_4/\text{Co}_9\text{S}_8$ spindles, and delivered a capacitance of 749 F g^{-1} .¹⁵ Very recently, CuCo_2S_4 nanoparticles have been synthesized in glycerol fulfills a capacitance of 5030 F g^{-1} at 20 A g^{-1} in a polysulfide electrolyte using a three-electrode system.¹⁶

Based on the above considerations, in this work, we successfully designed CuCo_2S_4 nanospheres on Ti wire for the first time prepared by a simple template-free hydrothermal method as a novel binder-free electrode for high-performance flexible coaxial fiber SC. The synergistic contributions from high density of active sites, rapid transfer of electrons and fast diffusion of ions lead the nanospheres-assembled SC to have a high specific capacitance and excellent rate capability.

Experimental

Fabrication of CuCo_2S_4 nanowires on Ti wire

Prior to deposition, commercial Ti wires were cleaned by sonication sequentially in acetone, 1 M HCl solution, deionized water, and ethanol for 15 min, respectively. After being dried, the Ti wire was transferred into Teflon-lined stainless autoclave. In a typical synthesis of CuCo_2O_4 nanosphere, 1 mmol $\text{CuCl}_2 \cdot 6\text{H}_2\text{O}$, 2 mmol $\text{CoCl}_2 \cdot 6\text{H}_2\text{O}$, 6 mmol NH_4F and 9 mmol

Key Laboratory of Catalysis and Materials Science of the State Ethnic Affairs Commission & Ministry of Education, South-Central University for Nationalities, Wuhan, Hubei Province, 430074, China. E-mail: Zhangdh27@163.com

† Electronic supplementary information (ESI) available. See DOI: 10.1039/c7ra04532h



$\text{CO}(\text{NH}_2)_2$ were dissolved in 30 mL deionized water by constant stirring. Then the solution was sealed in a Teflon-lined stainless-steel autoclave and kept at 120 °C for 6 h. After the reaction cooled to room temperature, the product was collected, washed, and then thermal treated at 300 °C for 3 h to obtain CuCo_2O_4 nanospheres. Finally, the obtained $\text{CuCo}_2\text{O}_4/\text{Ti}$ wire was immersed in 1 g Na_2S with 25 mL distilled water solution and kept at 140 °C for 10 h. After cooling slowly to room temperature, the Ti wire covered CuCo_2S_4 nanospheres was washed several times under deionized water and ethanol, then dried under vacuum at 60 °C for 8 h.

Three-electrode electrochemical measurements

As-prepared $\text{CuCo}_2\text{S}_4/\text{Ti}$ wire was used as the working electrode directly, a platinum electrode, and a saturated calomel electrode (SCE) were used as counter electrode and reference electrode, respectively. The electrochemical test was carried out in 3 M KOH electrolyte solution.

Fabrication of flexible all-solid-state coaxial SC

PVA/KOH gel electrolyte was prepared by mixing 6 g PVA (polyvinyl alcohol) and 3 g KOH with 60 mL deionized water and heated to 95 °C under vigorous stirring until it became clear. The electrodes were coated with the PVA/KOH and dried at 45 °C for 1 h. The final coaxial fiber SC was formed by wrapping the gel-coated CuCo_2S_4 electrode around the other gel-coated CuCo_2S_4 electrode.

Characterization

The synthesized products were characterized with an X-ray diffractometer. The morphology of the samples was characterized by scanning electron microscopy (SEM) and transmission electron microscopy (TEM). Cyclic voltammetry (CV), electrochemical impedance spectroscopy (EIS), and galvanostatic charge/discharge measurements were carried out on an electrochemical workstation (Ivium, CompactStat. 10800).

Calculation

The capacitance values were calculated from the discharge curve based on equation:

$$C_A = I \times \Delta t / (A \times \Delta V) \text{ (mF cm}^{-2}\text{)} \quad (1)$$

where ΔV is the potential drop during discharge (in V), I is the discharge current density (mA), Δt is discharge time (in seconds), A is the area of the coaxial SC (in cm). The electrochemical performance of device shown in the Ragone plot was based on the areal capacitance and measured from the discharge curves. The energy density and power density of the device was obtained from the equations:

$$E = C_A \times \Delta V^2 / 7200 \quad (2)$$

$$P = E \times 3600 / \Delta t \quad (3)$$

where E is the energy density (in W h cm^{-2}), and P is the power density (in W cm^{-2}).

Results and discussion

In this work, CuCo_2S_4 was developed on Ti fiber by the following two steps: (1) the CuCo_2O_4 nanosphere was hydrothermally grown on highly conductive Ti wire; (2) the hydrothermal treatment of such CuCo_2O_4 in the presence of Na_2S lead to CuCo_2S_4 *via* an anion-exchange reaction. The crystallographic structures of CuCo_2S_4 was characterized by X-ray power diffraction (XRD). All diffraction patterns reveal the successful formation of the carrollite structure phase of CuCo_2S_4 (according to the JCPDS card no. 42-1450), as shown in Fig. 1a. The main diffraction peaks appear at 26.6, 31.3, 38, 47, 50, and 54.8 respectively correspond to the (022), (113), (004), (224) (115) and (044) planes of the carrollite phase of the CuCo_2S_4 structure. The XRD pattern of CuCo_2O_4 was shown in Fig. S1.† To gain further information on the structure and composition of CuCo_2S_4 , we resort to X-ray photoelectron spectroscopy (XPS) measurement and the results is shown in Fig. 1b–d.

The spin-orbit doublet corresponding to Cu $2p_{1/2}$ and Cu $2p_{3/2}$ is readily observed in the Cu 2p region at 952.2 and 932.3 eV ($\Delta E = 19.9$ eV), respectively. As regards the Co 2p XPS spectrum of CuCo_2S_4 , it shows a doublet containing a low energy band (Co $2p_{3/2}$) and a high energy band (Co $2p_{1/2}$) at 781.1 and 796.3 eV (Fig. 1), consistent with the results reported elsewhere.¹⁷ The spin-orbit splitting value of Co $2p_{1/2}$ and Co $2p_{3/2}$ is over 15 eV, suggesting the coexistence of Co^{2+} and Co^{3+} .¹⁸ In the S 2p spectrum of CuCo_2S_4 , the peak at 162.4 and 161.3 eV are characteristics of S^{2-} ,¹⁹ and the component 169.2 eV can be ascribed to the sulphur in low coordination at the surface.²⁰ According to the XPS analysis, the near-surface of the CuCo_2S_4 sample has a composition of Co^{2+} , Co^{3+} , Cu^{2+} , Cu^{3+} , and S^{2-} , which is in good agreement with the CuCo_2S_4 .

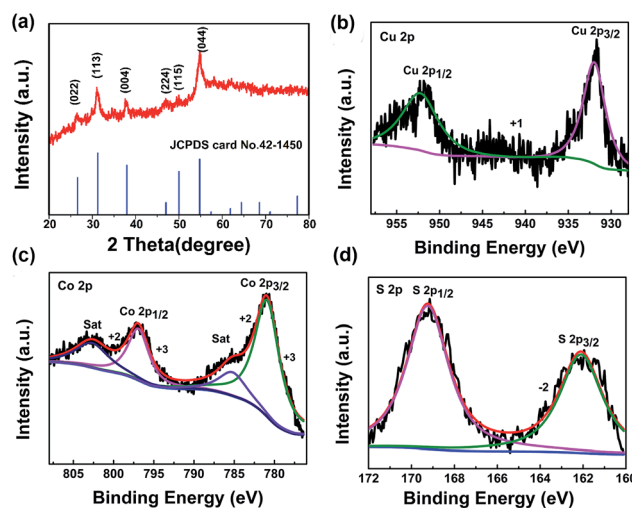
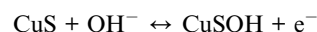


Fig. 1 (a) XRD pattern of the as-prepared CuCo_2S_4 , (b–d) XPS spectra of Cu 2p, Co 2p and S 2p, respectively.



The morphologies of the CuCo_2O_4 and CuCo_2S_4 were investigated by SEM and TEM, as shown in Fig. 2. It can be seen that the Ti wire was covered by spherical CuCo_2O_4 sample with diameter of about 15–20 μm (Fig. 2a and b). Typical the CuCo_2O_4 micro-spheres are composed of numerous small nanowires radially grown from the center. To better understand the formation mechanism of the as-synthesized urchin-like CuCo_2O_4 nanostructures on Ti wire, we carried out an additional experiment by reducing the molar of urea to 7 mmol, the corresponding SEM is shown in Fig. S2,[†] from which we can see nanowires and spheres were both found. Based on the result, it is manifested that the spheres were evolved from nanowires. After being treated with Na_2S , the obtained CuCo_2S_4 can well maintain the spheres nanostructures (Fig. 2c and d). The mass loading of CuCo_2O_4 on Ti wire is 0.36 and 0.5 mg cm^{-2} when the urea is 7 mmol and 9 mmol, respectively. It was expected that unique structure might have large surface area that could provide high specific capacitance due to the easy access of the active material in the redox process to their interface. More details of the morphological and structural features of the as-obtained sphere-like CuCo_2S_4 nanostructures are studied by HRTEM and selected-area electron diffraction (SAED). Fig. 2e exhibits the inter-planar spacing of 0.17 and 0.28 nm, which are consistent with the (004) and (113) planes of CuCo_2S_4 . Selected area electron diffraction (SAED) pattern of CuCo_2S_4 in Fig. 2f confirms that the CuCo_2S_4 nanospheres are of polycrystalline nature. According to the results, a possible mechanism is proposed. When the CuCo_2O_4 reacted with S^{2-} , HS^- , and H_2S in Na_2S solution, the ion-exchange reaction occurs slowly to convert all of the CuCo_2O_4 to CuCo_2S_4 and keep the morphology. The photos of pure Ti wire, $\text{CuCo}_2\text{O}_4/\text{Ti}$ and $\text{CuCo}_2\text{S}_4/\text{Ti}$ were demonstrated in Fig. S3,[†] respectively.

Regarding with such sphere-like nanostructure of Cu–Co sulfides, which are almost composed of surfaces with the most active sites exposed outside for the highly surface related faradaic reactions, their potential applications in pseudocapacitors are studied. Fig. 3a shows the cyclic voltammogram (CV) curves at different scan rates between -0.2 to 0.45 V. The redox peaks are derived from reversible faradaic reactions including following equations.



To further investigated the electrochemical performance of CuCo_2S_4 electrode, the galvanostatic charge/discharge measurements were conducted at different current densities between -0.2 to 0.45 V (Fig. 3b), the charge/discharge curves of CuCo_2S_4 show some curvature, which is due to redox transitions and corresponds to the typical redox couples in the CV curves.

The practical performance of the electrode in a full-cell setup was further evaluated by fabricating a CuCo_2S_4 -based flexible coaxial fiber SC. Fig. 3c shows the CV curves under different scan rates between 0 to 1 V. Galvanostatic charge/discharge curves of the flexible coaxial fiber SC at a set of current densities were further illustrated in Fig. 3d. The internal resistance (IR) drop versus current density are plotted in Fig. S4,[†] and corresponding linear functions are fitted. The small slope values demonstrate the low resistance of the as-fabricated SC. Fig. 3e shows the CV curves at a scan rate of 10 mV s^{-1} of CuCo_2O_4 and CuCo_2S_4 based flexible fiber SC, respectively. The integrated CV area for the CuCo_2S_4 fiber SC is significantly larger, this confirms that the CuCo_2S_4 nanosphere based electrodes are superlative for pseudocapacitive devices. We have also measured the charge transport and ion diffusion of two-electrode materials using electrochemical impedance spectroscopy (EIS), as shown in Fig. 3f, which reveals that the CuCo_2S_4 shows a much smaller R_{ct} in the Nyquist plots as compared to that of the CuCo_2O_4 . The results clearly

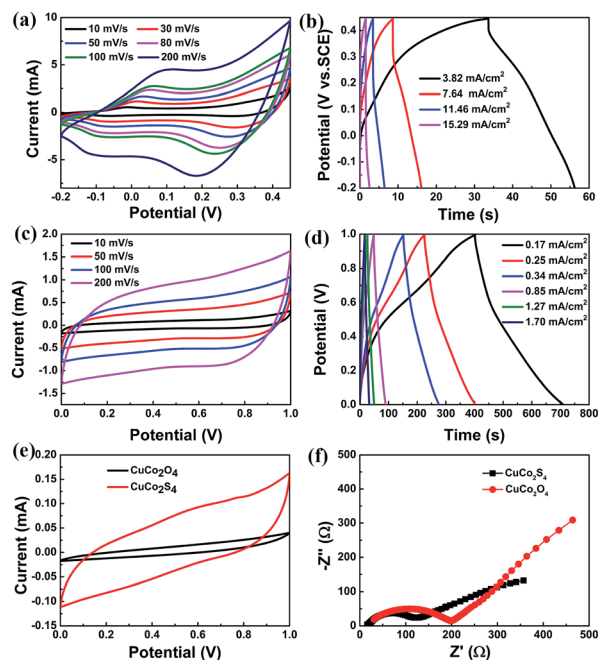


Fig. 3 (a and b) CV curves and galvanostatic charge/discharge curves of CuCo_2S_4 electrode in 3 M KOH electrolyte between -0.2 to 0.45 V. (c and d) CV curves and galvanostatic charge/discharge curves of as-fabricated flexible coaxial fiber SC device between 0 to 1 V. (e and f) The comparison of CV curve at 10 mV s^{-1} and EIS curve for flexible fiber SC based on CuCo_2O_4 and CuCo_2S_4 electrodes, respectively.

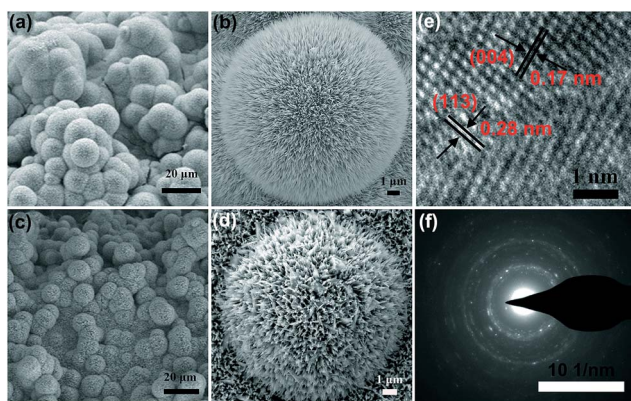


Fig. 2 SEM images of CuCo_2O_4 (a and b), (c and d) CuCo_2S_4 . (e) HRTEM image, (f) SAED pattern of CuCo_2S_4 .



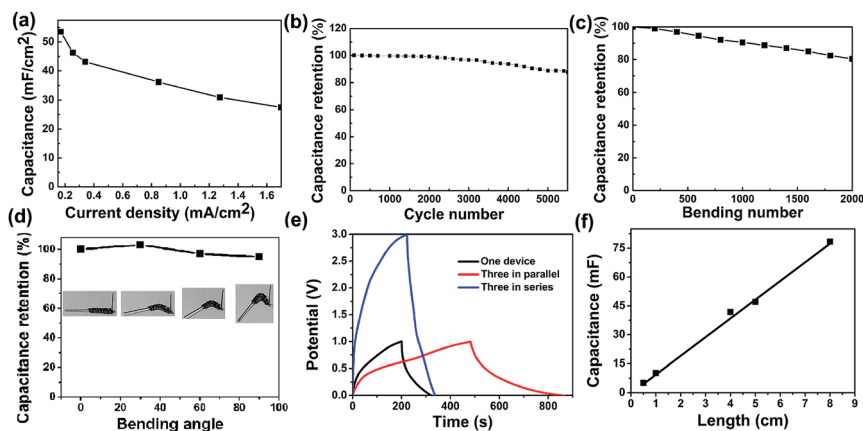


Fig. 4 (a) Areal capacitances as a function of current. (b) Capacitance retention versus cycle number. (c) Capacitance retention versus bending number. (d) Capacitance retention versus bending angles. Inset is the photos of fiber SC at different bending angles. (e) Galvanostatic charge/discharge curves for the fiber SCs with different configuration at a fixed current of 0.34 mA cm^{-2} . (f) Capacitance versus electrode length for fiber SCs.

demonstrate that the CuCo_2S_4 display favorable charge-transfer kinetics and fast electron transport and thus exhibit the dramatically enhanced pseudocapacitive performance.

The specific capacitance values are calculated to be approximately at 53.5 mF cm^{-2} at 0.17 mA cm^{-2} , which are much higher than $\text{MnO}_2/\text{graphene}$ ASC (4.57 mF cm^{-2}),²¹ $\text{MnO}_2/\text{CF}/\text{MoO}_3$ ASC (4.86 mF cm^{-2}),²² $\text{CNT}@/\text{Co}_3\text{O}_4$ yarns SC (52.6 mF cm^{-2}),²³ NiCo_2O_4 NG@CF (25.03 mF cm^{-2}).²⁴ Fig. 4b shows the capacitance retention evaluated at 0.34 mA cm^{-2} , after 5500 cycles, the capacitance retention is about 86% of the initial capacitance. The capacitance retention versus bending at 30° for 2000 cycles and bending different angles of the fiber SC is demonstrated in Fig. 4c and d, respectively. The results indicate the fiber SC has good flexibility and mechanical stability. Fig. 4e shows GCD curves of three SCs connected in parallel and in series. As compared with a single SC, the discharge time of the assembled parallel devices is about three times longer than that of a single device, which means approximately triple capacitance could be achieved. For three SCs combined in series, under the similar discharge time, the output voltage of this device can be extended to 3 V. Overall, these results illustrate that electrical performances of the series and parallel combinations of the SC devices, which show a good agreement with the theoretical models of series and parallel combined circuits, enabling them to combine multiply for practical applications. In Fig. S5,[†] the galvanostatic charge–discharge curves of the fiber SC with different length were shown. The calculated length specific capacitance has an approximately linear increase with the length increase of fiber SC (Fig. 4f), indicating the uniformity and the promising potential of large-scale fabrication of CuCo_2S_4 nanosphere fiber for flexible energy storage. Ragone plot (power density vs. energy density) of the flexible coaxial fiber SC describing was obtained and shown in Fig. S6.[†] The energy density decreased from 7.29 to $3.55 \mu\text{W h cm}^{-2}$, compared to the power density increased from 0.08 to 0.82 mW cm^{-2} , which is higher than that of those reported SC values.^{21–24}

Conclusions

In summary, we report the synthesis of sphere-like CuCo_2S_4 nanostructure on flexible Ti wire for the first time *via* a two-step hydrothermal method. In this unique nanoarchitecture, the CuCo_2S_4 spheres act as an excellent pseudocapacitive material that can be capable of fast electron conduction and ion diffusion. The as-fabricated flexible coaxial fiber SC based on CuCo_2S_4 micro-sphere exhibited a high specific capacitance of 53.5 mF cm^{-2} , good rate capability, as well as excellent cycling life.

Acknowledgements

We gratefully acknowledge the financial support of Hubei Province Natural Science Fund for Distinguished Young Scientists (2014CFA037) and the Central College Fund (CZQ16004).

Notes and references

- (a) D. Qi, Y. Liu, Z. Liu, L. Zhang and X. Chen, *Adv. Mater.*, 2017, **29**, 1602802; (b) L. B. Liu, Y. Yu, C. Yan, K. Li and Z. J. Zheng, *Nat. Commun.*, 2015, **6**, 7260; (c) Y. Yang, Q. Y. Huang, L. Y. Niu, D. R. Wang, C. Yan, Y. Y. She and Z. J. Zheng, *Adv. Mater.*, 2017, 1606679, DOI: 10.1002/adma.201606679; (d) Y. B. Zhang, B. Wang, F. Liu, J. P. Cheng, X. W. Zhang and L. Zhang, *Nano Energy*, 2016, **27**, 627.
- X. Li, L. Y. Zhang, N. Li, T. Yi and Z. Q. Liu, *Adv. Mater.*, 2016, **28**, 7680–7687.
- Y. M. Li, Y. S. Jiang, X. M. Sun, B. J. Wang and H. S. Peng, *Adv. Mater.*, 2016, **28**, 8431–8438.
- M. Zhu, Y. Huang, Y. Huang, H. Li, Z. Wang, Z. Pei, Q. Xue, H. Geng and C. Zhi, *Adv. Mater.*, 2017, 1605137.
- Y. Q. Zhu, C. B. Cao, S. Tao, W. S. Chu, Z. Y. Wu and Y. D. Li, *Sci. Rep.*, 2014, **4**, 5787.
- Y. Q. Fan, G. J. Shao, Z. P. Ma, G. L. Wang, H. B. Shao and S. Yan, *Part. Part. Syst. Charact.*, 2014, **31**, 1079–1083.



- 7 W. C. Xu, Y. Q. Liang, Y. G. Su, S. L. Zhu, Z. D. Cui, X. J. Yang, A. Inoue, Q. Wei and C. Y. Liang, *Electrochim. Acta*, 2016, **211**, 891–899.
- 8 J. Xiao, L. Wan, S. Yang, F. Xiao and S. Wang, *Nano Lett.*, 2014, **14**, 831.
- 9 R. J. Zou, Z. Y. Zhang, M. F. Yuen, J. Q. Hu, C. S. Lee and W. J. Zhang, *Sci. Rep.*, 2015, **5**, 7862.
- 10 Z. M. Zhang, Q. Wang, C. J. Zhao, S. D. Min and X. Z. Qian, *ACS Appl. Mater. Interfaces*, 2015, **7**, 4861.
- 11 L. Yu, L. Zhang, H. B. Wu and X. W. Lou, *Angew. Chem., Int. Ed.*, 2014, **53**, 3711–3714.
- 12 Y. M. Gao, L. W. Wei, W. T. Cui, S. Z. Zheng, Z. Hou and H. W. Chen, *ACS Appl. Mater. Interfaces*, 2015, **7**, 4311–4319.
- 13 J. Yang, Y. Zhang, C. Sun, G. Guo, W. Sun, W. Huang, Q. Yan and X. Dong, *J. Mater. Chem. A*, 2015, **3**, 11462–11470.
- 14 J. W. Xiao, L. Wan, S. H. Yang, F. Xiao and S. Wang, *Nano Lett.*, 2014, **14**, 831–838.
- 15 L. R. Hou, Y. Y. Shi, S. Q. Zhu, M. Rehan, G. Pang, X. G. Zhang and C. Z. Yuan, *J. Mater. Chem. A*, 2017, **5**, 133–144.
- 16 J. Tang, Y. Ge, J. Shen and M. Ye, *Chem. Commun.*, 2016, **52**, 1509–1512.
- 17 J. Xiao, X. Zeng, W. Chen, F. Xiao and S. Wang, *Chem. Commun.*, 2013, **49**, 11734.
- 18 J. Xu, P. Gao and T. S. Zhao, *Energy Environ. Sci.*, 2012, **5**, 5333.
- 19 Q. Wang, L. Jiao, H. Du, Y. Si, Y. Wang and H. J. Yuan, *Mater. Chem.*, 2012, **22**, 21387.
- 20 H. Chen, J. Jiang, L. Zhang, H. Wan, T. Qi and D. Xia, *Nanoscale*, 2013, **5**, 8879.
- 21 N. Yu, H. Yin, W. Zhang, Y. Liu, Z. Y. Tang and M. Q. Zhu, *Adv. Energy Mater.*, 2016, **6**, 1501458.
- 22 J. Noh, C. M. Yoon, Y. K. Kim and J. Jang, *Carbon*, 2017, **116**, 470–478.
- 23 F. H. Su, X. M. Lv and M. H. Miao, *Small*, 2015, **11**(7), 854–861.
- 24 S. T. Senthilkumar, N. Q. Fu, Y. Liu, Y. Wang, L. M. Zhou and H. T. Huang, *Electrochim. Acta*, 2016, **211**, 411–419.

